High CD8 T-Cell Receptor Clonality and Altered CDR3 Properties Are Associated With Elevated Isolevuglandins in Adipose Tissue During Diet-Induced Obesity

Wyatt J. McDonnell,[1,2,3] John R. Koethe,[2,4,5] Simon A. Mallal,[1,2,4,6] Mark A. Pilkinton,[2,4,5] Annet Kirabo,[7] Magdalene K. Ameka,[8] Matthew A. Cottam,[8] Alyssa H. Hasty,[5,8] and Arion J. Kennedy[8]

Diabetes 2018;67:2361–2376 | https://doi.org/10.2337/db18-0040

Adipose tissue (AT) CD4$^+$ and CD8$^+$ T cells contribute to obesity-associated insulin resistance. Prior studies identified conserved T-cell receptor (TCR) chain families in obese AT, but the presence and clonal expansion of specific TCR sequences in obesity has not been assessed. We characterized AT and liver CD8$^+$ and CD4$^+$ TCR repertoires of mice fed a low-fat diet (LFD) and high-fat diet (HFD) using deep sequencing of the TCRβ chain to quantify clonal expansion, gene usage, and CDR3 sequence. In AT CD8$^+$ T cells, HFD reduced TCR diversity, increased the prevalence of public TCR clonotypes, and selected for TCR CDR3 regions enriched in positively charged and less polarized amino acids. Although TCR repertoire alone could distinguish between LFD- and HFD-fed mice, these properties of the CDR3 region of AT CD8$^+$ T cells from HFD-fed mice led us to examine the role of negatively charged and nonpolar isolevuglandin (isoLG) adduct-containing antigen-presenting cells within AT. IsoLG-adducted protein species were significantly higher in AT macrophages of HFD-fed mice; isoLGs were elevated in M2-polarized macrophages, promoting CD8$^+$ T-cell activation. Our findings demonstrate that clonal TCR expansion that favors positively charged CDR3s accompanies HFD-induced obesity, which may be an antigen-driven response to isoLG accumulation in macrophages.

The stromal vascular fraction (SVF) of adipose tissue (AT) contains immune cells that contribute to the paracrine signaling milieu that modulates local inflammation and adipocyte function (1). This has been posited to be the primary mechanism by which inflamed AT induces insulin resistance (IR) because inflammatory cytokines are known to interfere with insulin signaling. AT macrophages (ATMs) are believed to serve as the primary cell type responsible for inflammation-induced IR, with AT T cells serving as modulators of ATM activation. However, additional evidence suggests that adaptive immune responses, mediated by both B cells (2,3) and T cells (4–7), also contribute directly to adverse changes in adipocyte metabolic fitness in obesity.

Regulatory T cells (Tregs) are reduced in obese AT compared with lean AT (6), are protective against AT inflammation and IR, and possess a distinctive gene repertoire (6). Experimental models using adoptive transfer of CD4$^+$ T cells into lymphocyte-free Rag1$^{-/-}$ mice reversed weight gain and IR, and depletion of CD8$^+$ T cells in AT reduced ATM density and improved insulin sensitivity. These findings suggest that immunotherapy could represent a novel approach to treatment of metabolic disease (4,8). Although the etiology of T-cell expansion is unclear at present, in vitro studies have found that obese fat independently activates CD8$^+$ T cells and induces proliferation, whereas lean fat has little effect (4).

Spectratyping analyses of AT CD8$^+$ T cells in the setting of obesity also have described a narrowed repertoire of T-cell receptor (TCR) Vα and Vβ chain families compared

[1]Department of Pathology, Microbiology and Immunology, Vanderbilt University School of Medicine, Nashville, TN
[2]Center for Translational Immunology and Infectious Disease, Vanderbilt University Medical Center, Nashville, TN
[3]Vanderbilt Vaccine Center, Vanderbilt University Medical Center, Nashville, TN
[4]Department of Medicine, Division of Infectious Diseases, Vanderbilt University Medical Center, Nashville, TN
[5]Veterans Administration Tennessee Valley Healthcare System, Nashville, TN
[6]Institute for Immunology and Infectious Diseases, Murdoch University, Murdoch, Western Australia, Australia
[7]Division of Clinical Pharmacology, Department of Medicine, Vanderbilt University Medical Center, Nashville, TN
[8]Department of Molecular Physiology and Biophysics, Vanderbilt University School of Medicine, Nashville, TN

Corresponding author: Arion J. Kennedy, arion.kennedy@vanderbilt.edu.

Received 21 January 2018 and accepted 20 August 2018.

This article contains Supplementary Data online at http://diabetes.diabetesjournals.org/lookup/suppl/doi:10.2337/db18-0040/-/DC1.

with cells in lean tissue, suggesting that these $CD8^+$ T cells may undergo oligoclonal expansion in AT (4,9). An important limitation of spectratyping is that it cannot detect individual TCRs, does not provide complementarity-determining region 3 (CDR3) sequences, and only describes deviations from the normally Gaussian distribution of amino acid or nucleotide length. Spectratyping also was used to demonstrate that proinflammatory $CD4^+$ T helper 1 (T_H1) cells with a biased TCR Vα repertoire expand in AT, but $CD4^+$ T_H17 cells do not (7). Furthermore, progressive reductions in $CD4^+FoxP3^+$ anti-inflammatory T cells with increasing obesity were detected (7). Although spectratyping in these studies has allowed the authors to suspect clonal expansion, it did not allow them to quantify TCR repertoire diversity, detect specific clones, examine CDR3 sequences and properties, or examine clonal overlap. Similarly, although analysis of CDR3α sequences from 98 single AT Tregs showed that AT Tregs have a unique V gene repertoire (6), the diversity observed and its relation to the native repertoire were less clear because the transgenic mice in this study only carried a single Vα gene, were designed to produce a distinctly narrowed TCR repertoire, and had a lower-than-normal thymic output (10).

Because prior studies demonstrated that obese mice have increased AT T-cell density and a shift toward a proinflammatory phenotype, we hypothesized that high-fat feeding would induce an increase in AT $CD4^+$ and $CD8^+$ T cells in conjunction with the clonal expansion of specific TCR clonotypes. We performed high-throughput TCR DNA sequencing of the AT and livers of mice fed either a high-fat diet (HFD) or a low-fat diet (LFD). The TCR repertoires of mice fed an HFD are markedly enriched for public clonotypes in the CD8 and CD4 TCR repertoires of the AT. This overlap in TCRs between HFD samples distinguished between lean and obese mice, suggesting selection both for more public clonotypes and for autoreactive T cells. We find that the $CD8^+$ TCR repertoire of mice fed an HFD is more clonal and characterized by more charged and less polar CDR3s. These HFD-induced features of the T-cell response led us to examine possible sources of neoantigens within AT, specifically the immunogenic and well-characterized isolevuglandin (isoLG) protein adducts, which are the sole lipid neoantigen species that induces a T-cell response in hypertension (11). We detected an increase in immunogenic isoLGs, a family of negatively charged protein adducts generated from reactive γ-ketoaldehydes, in CD206-expressing macrophages isolated from AT of HFD-fed mice. Moreover, isoLGs were elevated in M2-polarized macrophages in vitro, and cocultures of these macrophages with T cells promoted $CD8^+$ T-cell activation. These observations demonstrate that dietary modifications affect the adaptive immune response in AT in a systemic fashion and provide novel insights into potential mechanisms by which HFD and obesity may lead to pathogenic T-cell responses directed toward modified self-peptides.

RESEARCH DESIGN AND METHODS

Mice and Diets

Male C57BL/6J mice were purchased from The Jackson Laboratory. Studies were divided into three cohorts. The first cohort was used for AT T-cell studies and TCR repertoire analysis, the second was used for isoLGs, and the third was used for measuring isoLGs in ATM subsets and coculture studies. At 8 weeks of age, mice were placed on a 10% LFD for 9 weeks. Subsequently, mice were randomized into either the LFD or the HFD group. Both diets were purchased from Research Diets (HFD: D12492, LFD: D12450B; New Brunswick, NJ). Mice were fed ad libitum and given free access to water. All animal procedures were performed with approval from the institutional animal care and use committee of Vanderbilt University.

Glucose Tolerance Testing

Mice were fasted for 5 h, and basal blood glucose levels were measured (0 min) before intraperitoneal administration of 1.5 g dextrose/kg lean body mass. Blood glucose was assessed at 15, 30, 45, 60, 90, and 150 min after injection.

AT SVF Isolation, Liver Nonparenchymal Cell Isolation, and FACS Analysis

AT SVF Isolation

The SVF was isolated from epididymal fat pads through collagenase digestion and differential centrifugation as previously described (12).

Liver Nonparenchymal Cell Isolation

Liver was excised and minced in 1 mg/mL collagenase in PBS. Minced liver was incubated on a shaker at 37°C for 30 min. The cell suspension was filtered and spun at 800*g* for 10 min at 4°C. The cell pellet was suspended in 33% Percoll. The Percoll gradient was centrifuged at 800*g* for 30 min at room temperature. Red blood cells were lysed using ammonium-chloride-potassium lysing buffer. Cells were centrifuged at 800*g* for 5 min at 4°C. The cells were suspended in FACS buffer and stained for flow cytometry. The following primary fluorophore-conjugated antibodies, along with isotype controls, were used to characterize AT and liver T-cell populations: PerCP-Cy5.5–conjugated anti-mouse CD45, antigen-presenting cell (APC)–conjugated anti-mouse TCRβ, Alexa Fluor 700–conjugated anti-mouse CD4, and V500-conjugated anti-mouse CD8a (all from eBioscience). DAPI was added immediately before analysis to enable discrimination between live and dead cells.

FACS Analysis

FACS was performed on a BD FACSAria III flow cytometer (BD Biosciences) at the Vanderbilt Medical Center Flow Cytometry Core shared resource, and data were analyzed using FlowJo software (Tree Star). The gating strategy is shown in Supplementary Fig. 1.

TCR Sequencing

Genomic DNA from sorted $CD4^+$ and $CD8^+$ T cells was isolated using the QIAamp DNA Blood Mini Kit (QIAGEN).

DNA from AT $CD4^+$ and $CD8^+$ T cells and liver $CD8^+$ T cells was used for bulk TCRβ CDR3 region amplification and sequencing using the ImmunoSEQ assay (Adaptive Biotechnologies, Seattle, WA). In this method, bias-controlled V and J gene primers are used to amplify rearranged V(D)J segments for sequencing (13).

IsoLG Adduct Quantification

ATMs were analyzed by flow cytometry using the following antibodies: PerCP-Cy5.5–conjugated anti-mouse CD64, PE-Cy7–conjugated anti-mouse CD86, Alexa Fluor 700–conjugated anti-mouse CD11c, PE-conjugated anti-mouse CD206, APC-conjugated anti-mouse F4/80, and PECF594-conjugated anti-mouse CD45 (Becton Dickinson). We used intracellular staining with the single-chain antibody D-11 to detect isoLG protein adducts. The D-11 single-chain variable fragment antibody was labeled with Alexa Fluor 488 using the APEX Alexa Fluor 488 Antibody Labeling Kit (Invitrogen). Cells labeled with surface antibodies were fixed and permeabilized for intracellular detection of isoLGs using the FIX & PERM Cell Fixation and Permeabilization Kit (Invitrogen). Dead cells were excluded from analysis using a LIVE/DEAD Fixable Dead Cell Stain Kit (Invitrogen). For each experiment, we gated on single live cells and used fluorescence minus one controls for each fluorophore to establish the gates. Data were analyzed using FlowJo software. The gating strategy is shown in Supplementary Fig. 2*A*.

Bone Marrow–Derived Macrophage Polarization and T-Cell Coculture

Bone marrow-derived macrophages (BMDMs) isolated from C57BL/6J mice were obtained as described by Trouplin et al. (14). On day 6, fully differentiated BMDMs were split and loaded into 24-well plates at a density of 700,000 cells per well in L929-conditioned media. Cells were allowed to adhere overnight and then polarized as follows: For M1 polarization, BMDMs were stimulated for 24 h with interferon-γ (100 ng/mL; R&D Systems) and lipopolysaccharide (10 ng/mL; Sigma). For M2 polarization, BMDMs were treated for 96 h with interleukin 4 (10 ng/mL; R&D Systems) and interleukin 13 (10 ng/mL; R&D Systems). For metabolic polarization (metabolically activated macrophages [MMes]), BMDMs were treated for 24 h with 30 mmol/L glucose, 10 nmol/L insulin, and 0.4 mmol/L palmitic acid as described by Hill et al. (15). For *tert*-butyl hydroperoxide (TBHP) treatment, BMDMs were treated with 1 mmol/L TBHP for 30 min, after which the TBHP media were replaced with fresh media. T cells were isolated from spleens of LFD- and HFD-fed mice using APC magnetic beads (Miltenyi) to isolate TCRβ-APC–labeled cells. Polarized BMDMs were cocultured with isolated pan-T cells from LFD- and HFD-fed mice at a ratio of 1:2. BMDMs and T cells were collected.

Immunostaining for flow cytometry was performed using the following antibodies: for macrophage panel, PE-conjugated anti-mouse CD45, APC-conjugated anti-mouse F4/80, and intracellular staining with the single-chain antibody D-11 to detect isoLG protein adducts, and for activated T-cell panel, PerCP-Cy5.5–conjugated anti-mouse CD45, fluorescein isothiocyanate–conjugated anti-mouse CD4, PECF594-conjugated anti-mouse CD69, and PE-Cy7–conjugated anti-mouse CD8 (BD Biosciences) and DAPI. The gating strategy for BMDMs is shown in Supplementary Fig. 3 and for activated T cells in Supplementary Fig. 4.

Computation

Data Import and Preprocessing

All TCR sequences, including nonproductive sequences, from immunoSEQ were processed and imported using VDJTools as previously described (16). Amino acid sequences were analyzed because the amino acid sequence of a TCR determines its structural properties.

Repertoire Similarity

VDJTools was used to calculate a pairwise distance matrix between samples using the geometric mean overlap $F_{ij} = \sqrt{f_{ij} f_{ji}}$, such that $f_{ij} = \sum_{k=1}^{N} \varnothing_{ik}$ sums to the frequencies of TCRs shared between two samples present in the first as the distance metric. This matrix was used to perform complete linkage hierarchical clustering through the hclust function in base R version 3.4.0 software. Permutation testing confirmed significant factors in clustering. Each sample was downsampled in a density-dependent fashion to 10,000 clonal sequences to confirm significant factors in clustering and significant structure. Mice with $<$1,000 clonotypes detected in any sample were excluded from analysis.

Repertoire Overlap

The VDJTools JoinSamples routine was used to detect clonotypes overlapping between samples with shared amino acid sequences.

Clonal Homeostasis

The frequency of each clonotype within each sample was calculated using VDJTools. The clonal space, defined by the sum of frequencies, occupied by the top 1–3, 4–10, 11–20, 21–50, 51–100, and bottom 101–*n* clonotypes was calculated per sample as described previously (17). These clonal bins were log-transformed and tested for differences in the ratio of their geometric means between LFD and HFD. The CD4 and CD8 clonal bins were then condensed per mouse and used as input for hierarchical clustering. Average linkage was used as the clustering method, and absolute correlation was used as the distance metric. For visualization, the geometric means for each set of samples was calculated per clonal bin and normalized to range from 0 to 1.

t-*Distributed Stochastic Neighbor Embedding*

Clonal homeostatic proportions were fed into the *t*-distributed stochastic neighbor embedding (*t*-SNE) algorithm with principal component analysis (PCA) before projection. Perplexity was set at 2, θ at 10^{-5}, and learning rate at 1, and perplexity was exaggerated for the first

50 iterations to restrain the *t*-SNE algorithm in a size-dependent fashion. Five thousand iterations were allowed. Calculations were performed using the Rtsne package (18).

PCA

Homeostatic proportions were centered and scaled before projection. Calculations were performed using the prcomp function in base R.

P *Value–Validated Clustering*

Clonal homeostatic proportions were clustered using complete linkage for clustering and absolute correlation for distance. Calculations were performed using the pvclust package of R (19).

Multidimensional Scaling

The pairwise distance matrix using geometric mean overlap was used as input for nonmetric multidimensional scaling using VDJTools (16) and the iso*MDS* function from the Modern Applied Statistics With S-PLUS package (20).

Repertoire Publicity Analysis

Public clonotypes were defined as those shared among at least three mice to account for sampling depth. All public clonotypes were retrieved using VDJTools (16), and the frequency within each mouse was converted to a binary value representing present (1) or absent (0). For each public clonotype, each dietary group was then assigned a binary value representing whether it was greater than (1), less than (0), or equally prevalent to (0) the other dietary group. These values were then used to construct a 2×2 contingency table representing the proportion of public TCRs for each dietary group, in similar fashion to analysis of concentration and association (21,22).

Sequence Logo Plots

Seq2Logo was used to generate three types of sequence logo plots. The median TCRβ length was calculated, and these sequences were used to generate logo plots using Shannon entropy (the probability of an amino acid appearing), the Kullback-Leibler divergence (probability with enrichment and depletion), and the probability-weighted Kullback-Leibler divergence (probability of each amino acid multiplied by its weight). Where indicated, Hobohm first algorithm (nearest-neighbor selection clustering) was used to bin TCRs with similar sequences, using a threshold of 20% to account for the diversity and divergence of the TCRβ chain. A weighted prior correction of 200 pseudocounts on the basis of the BLOSUM62 matrix was used to correct for amino acids detected at very low levels as previously described (23). Where appropriate, each mouse's TCR repertoire also was down-sampled in density-dependent fashion to 10,000 clonal sequences to draw comparisons between samples and to cross-validate the multidimensional structure and similarity of data.

Statistics

Significance was set a priori at $P < 0.05$.

Weight and Clonality

Repeated-measures ANOVA with Bonferroni multiple comparisons testing was used to assess changes between diet groups using GraphPad Prism version 6.05 software (GraphPad Software, La Jolla, CA) and R version 3.4.0 (RStudio version 1.0.143).

Glucose Tolerance Testing

Two-way ANOVA with post hoc Bonferroni-Šídák multiple comparisons testing was used to assess differences between dietary groups at each time point.

Clonal Homeostasis

The Mann-Whitney *U* test was used to assess differences in the geometric mean ratios of clonal homeostasis bins using GraphPad Prism software.

Factor Analysis in Clustering

Significant factors in hierarchical clustering were assessed using permutation testing in VDJTools for repertoire similarity.

Cluster Analysis in Clonal Homeostasis

Cluster significance for clonal homeostatic signatures was assessed using multistep-multiscale bootstrap resampling in the pvclust package of R (19).

CDR3 Amino Acid and Nucleotide Profiling

CDR3 properties were calculated per sample and per dietary group using VDJTools (16). The Mann-Whitney *U* and Wilcoxon signed rank tests were used to assess differences in CDR3 properties using GraphPad Prism and R software. *P* values were corrected using the Benjamini-Hochberg false discovery rate correction.

Repertoire Publicity

We tested the 2×2 contingency table computed as described above using Pearson χ^2 test. The *P* value for this test was calculating using Monte Carlo simulation with 1,000 bootstraps in R. *P* values were adjusted using the Bonferroni correction to control the familywise error rate.

RESULTS

High-Fat Feeding Reduces CD8+ T-Cell Diversity in AT

An HFD increased body weight (Supplementary Fig. 5*A*), AT mass (Supplementary Fig. 5*B*), and liver mass (Supplementary Fig. 5*C*). Although fasting blood glucose was similar among diet groups (Supplementary Fig. 5*D*), plasma insulin was significantly higher in the HFD-fed mice (Supplementary Fig. 5*E*), and HFD-fed mice had impaired glucose tolerance (Supplementary Fig. 5*F*). We next compared the T-cell density (cells/gram tissue) in AT and liver. Similar to previous studies (4), the density of AT $CD8^+$ T cells was elevated by threefold in HFD-fed mice compared with LFD-fed controls (Fig. 1*A*). In contrast, AT $CD4^+$ T-cell and liver $CD8^+$ T-cell populations were not significantly different between groups (Fig. 1*B* and *C*).

TCRβ chain amplification and deep sequencing of AT $CD8^+$ and $CD4^+$ T cells as well as liver $CD8^+$ T cells yielded

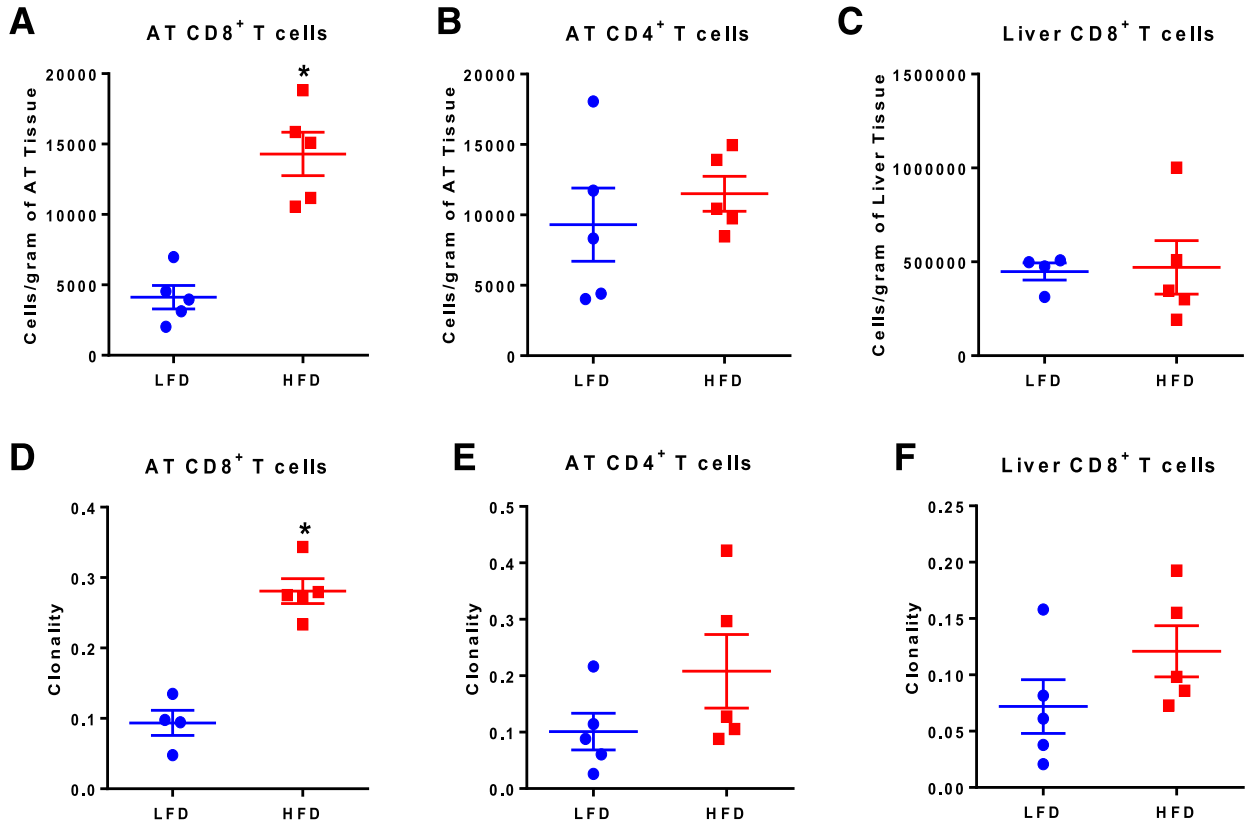

Figure 1—HFD leads to increased T-cell number and clonality. *A* and *B*: AT CD8$^+$ number was increased in HFD mice (two-tailed *t* test) (*A*), whereas CD4$^+$ T cells were not significantly increased (*B*). *C*: There was no difference in the number of liver CD8$^+$ T cells. *D*: The TCR repertoires of AT CD8$^+$ T cells of HFD-fed mice are significantly more clonal than those of LFD-fed mice ($P < 0.05$, two-tailed Student *t* test). *E*: AT CD4$^+$ clonality did not differ between HFD and LFD ($P = 0.18$, two-tailed Student *t* test). *F*: Liver CD8$^+$ T cells of HFD-fed mice are not significantly clonal compared with LFD-fed mice ($P = 0.18$, two-tailed Student *t* test). Data points represent the clonality of each mouse as calculated using normalized Shannon entropy. Data are mean ± SEM (n = 4–5 mice/group). *$P \leq 0.05$.

three repertoires of V(D)J gene TCR sequences per mouse. These TCR sequences were used to calculate overall repertoire clonality as measured by Shannon entropy using the immunoSEQ Analyzer. AT CD8$^+$ T cells from HFD-fed mice had a higher clonality score, indicating less diversity, compared with LFD-fed mice (Fig. 1*D*). Although there was somewhat increased clonality in AT CD4$^+$ T cells (Fig. 1*E*) and liver CD8$^+$ T cells (Fig. 1*F*), this difference was not significant; because we did not detect differences in the liver CD4$^+$ populations, we did not sequence these T cells.

T-Cell Clonal Distributions Differ Between Mice Fed an HFD or LFD

Our observation of the marked clonality in the CD8$^+$ T cells from AT of HFD-fed mice led us to ask whether diet-induced obesity (DIO) affected the relative contributions of the major and minor clonotypes within a given TCR repertoire. We first examined this clonal homeostatic space within each mouse using the Mann-Whitney *U* test after downsampling to account for sampling depth. The top clonotypes of mice fed an HFD occupied significantly higher proportions of clonal space ($P < 0.001$) (Fig. 2*A*), whereas the bottom clonotypes occupied significantly less clonal space ($P < 0.001$) in CD8$^+$ T cells from AT and liver. The proportions of these TCRs from the AT and liver also distinguish between lean and obese mice on the basis of *t*-SNE (Fig. 2*B*), PCA (Fig. 2*C*), and hierarchical clustering ($P < 0.05$) (Fig. 2*D*). These multidimensional analyses demonstrate that HFD distorts the size of the largest and smallest clonotypes of the repertoire, an observation that traditional measures of clonality, such as Shannon entropy, do not capture.

Shared Clonotypes and Gene Usage Distinguish Between TCR Repertoires From Mice Fed LFD or HFD

Hierarchical clustering on repertoire similarity of TCR clonotypes sharing the same amino acid sequence successfully distinguished between both AT CD8$^+$ TCR ($P < 0.05$) and AT CD4$^+$ TCR repertoires of LFD- and HFD-fed mice ($P < 0.001$) (Fig. 3*A*). The impact of dietary group on repertoire similarity held true when pooling TCR repertoires from AT and liver and from both CD8$^+$ and CD4$^+$ T cells ($P = 0.01$) (Fig. 3*B*). Expansion of both major and minor clonotypes led to synchronous changes in CD8$^+$ T cells between AT and liver repertoires within each mouse (Fig. 3*C* and Supplementary Table 1) in a diet-dependent fashion ($P < 0.05$). Each mouse's AT and liver repertoires were most similar to each other, demonstrating the reproducibility of repertoire changes that are tissue specific.

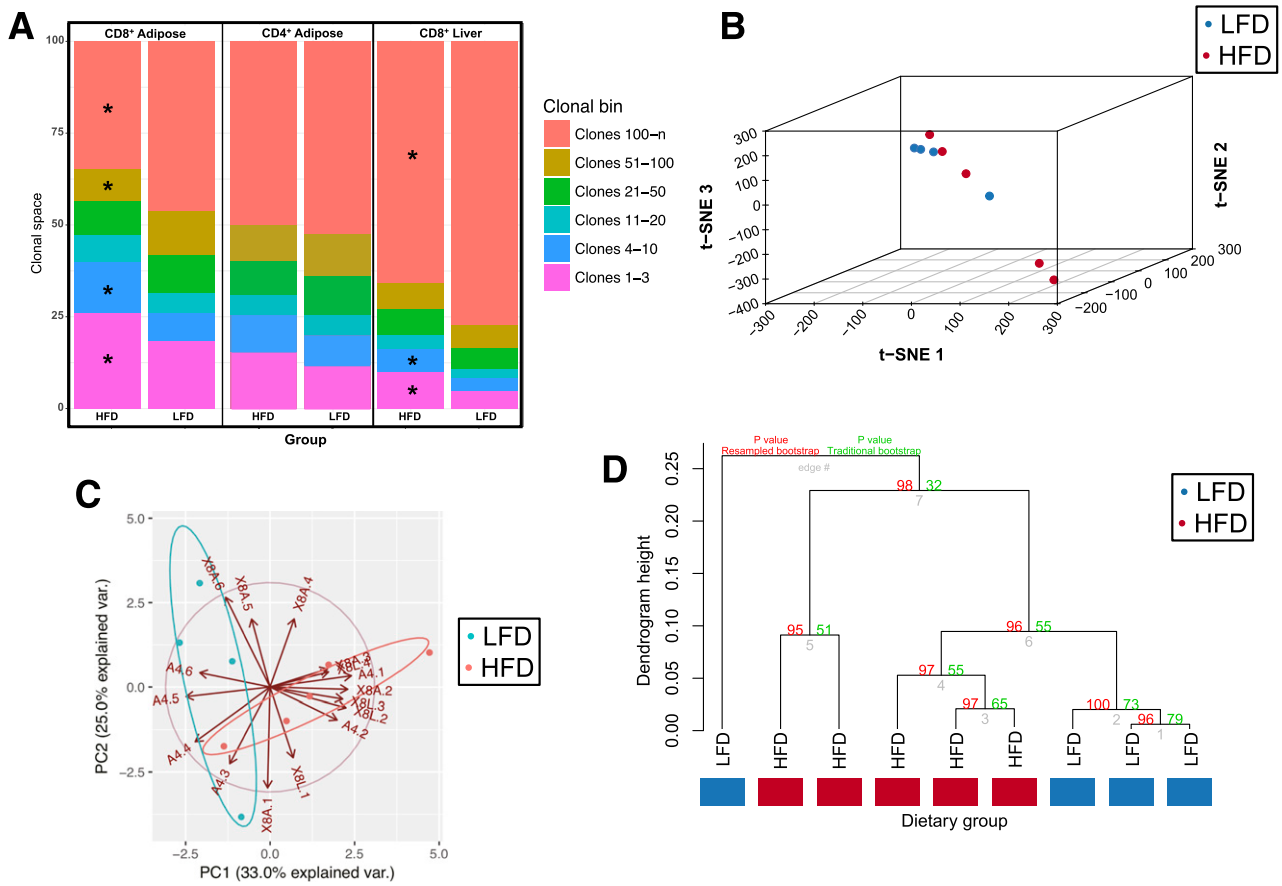

Figure 2—Clonal homeostatic space differs between dietary groups and is a distinctive signature in multidimensional space. *A*: The space within the repertoire occupied by the clonotypes within each clonal bin was calculated for each mouse. The geometric mean for each of these proportions was calculated for each diet group, and the clonal homeostatic proportions occupied were tested using the two-tailed Mann-Whitney *U* test. The clonal proportions distinguish between dietary conditions using modern machine learning methods measuring several multidimensional distances. *B*: Two dimensional *t*-SNE projection of clonal homeostatic proportions from the AT reveals that lean and obese mice differ in clonal homeostasis as measured in a two-dimensional projection. PCA with centering and scaling was performed before *t*-SNE, and 15 dimensions were retained for embedding with the *t*-SNE algorithm. *C*: PCA projection of clonal homeostatic proportions reveals that the repertoire space occupied by both highly and lowly abundant clonotypes distinguishes between lean and obese mice. *D*: Hierarchical clustering using average linkage and absolute correlation reveals that clonal homeostatic proportions distinguish between lean and obese mice. Values shown at each node demonstrate the confidence that a cluster truly exists as measured using multiscale bootstrap resampling and traditional bootstrapping. Multiscale bootstrap resampling validates that these characteristic differences are not expected to distinguish between lean and obese mice by chance alone. *$P \leq 0.05$. PC, principal component; var., variance.

Our observation of the dissimilarity of the TCR repertoires between dietary groups led us to examine whether Vβ gene usage differed in AT between LFD- and HFD-fed mice. The AT CD8$^+$ T-cell repertoires of each dietary group demonstrated differential usage of several Vβ genes (Fig. 4*A*). Neither LFD nor HFD affected Jβ gene usage in the AT (Fig. 4*B*). Similar to other groups, we observed differential Vβ gene usage between CD4$^+$ and CD8$^+$ T cells (24,25), which also distinguished between CD4$^+$ and CD8$^+$ TCR repertoires (Supplementary Fig. 6). CD4$^+$ TCRs expressed a decrease in charge and increase in polarity compared with CD8$^+$ TCRs ($P < 0.05$) (Supplementary Fig. 7*A*). They also had characteristically shorter N-D gene-N regions ($P < 0.05$) (Supplementary Fig. 7*B*).

HFD Increases the Prevalence of Public T-Cell Clonotypes

The observation that diet strongly influences TCR repertoire similarity led us to ask whether HFD-fed mice were more likely to share clonotypes than LFD-fed mice. To test this hypothesis, we used a specialized Monte Carlo–validated χ^2 test (Supplementary Fig. 8). This test proved to be robust to both *P* value permutation and probability proportionate to size downsampling in addition to extremely conservative *P* value correction. HFD mice were more likely to have public clonotypes shared among at least three mice in their CD8$^+$ ($P < 0.001$) and CD4$^+$ AT T-cell repertoires ($P = 0.01$). This difference was not observed in the liver CD8$^+$ TCR repertoire.

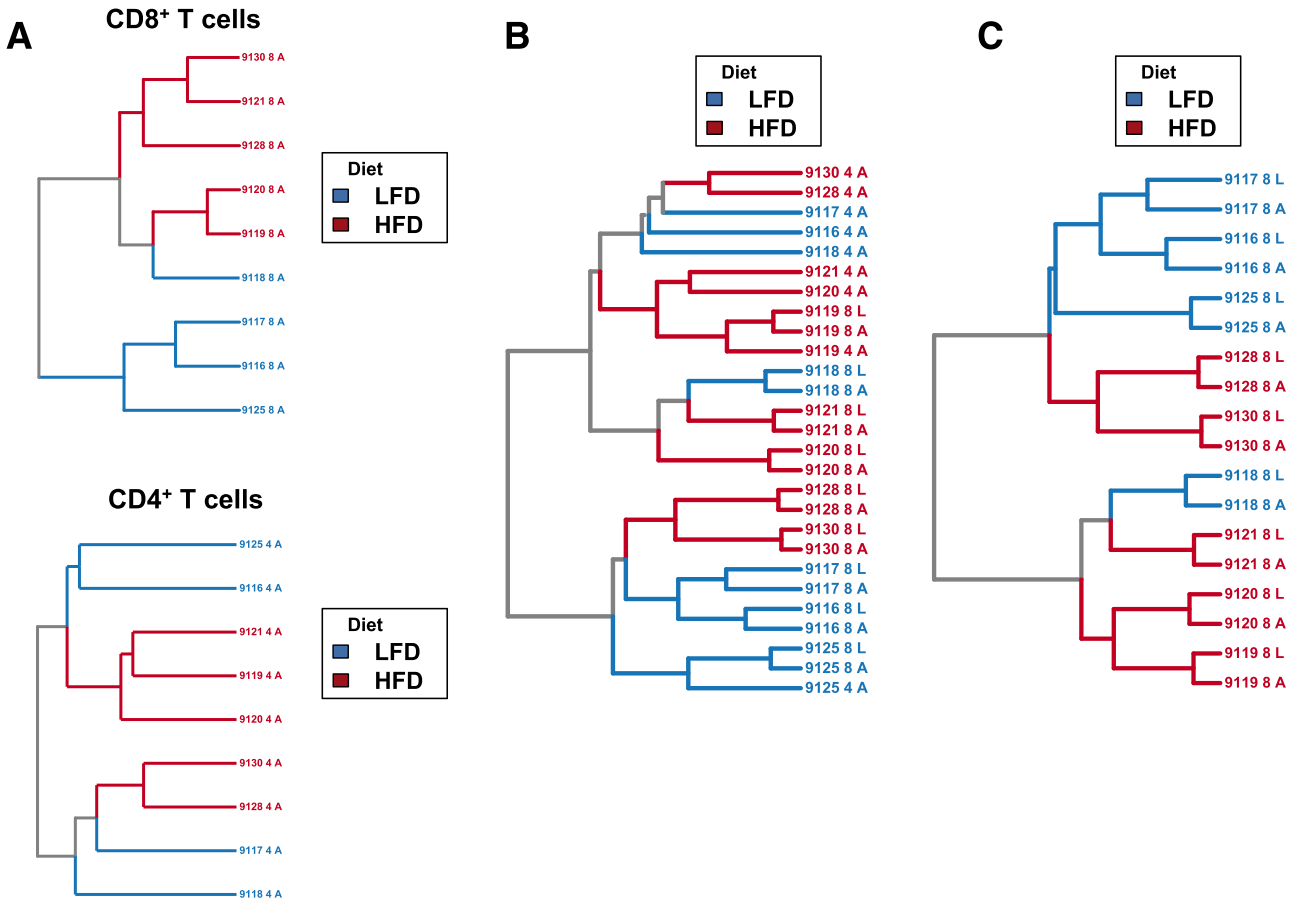

Figure 3—Dietary group is predictive of repertoire similarity and synchronously alters the TCR repertoire in AT. Geometric mean overlap was used to calculate pairwise distance matrices on the basis of shared clonotypes with identical CDR3 amino acid sequences. Labels on each dendrogram correspond to a specific mouse, tissue type, and cell type (4 or 8). *A*: AT $CD8^+$ (upper) and $CD4^+$ repertoires (lower) share more TCRs within diet groups than between diet groups ($P < 0.0001$ for $CD8^+$ and $CD4^+$, permutation of pairwise distance matrix). This suggests that sets of shared TCRs are enriched and depleted in a diet-dependent fashion. *B*: Diet significantly affects repertoire similarity across multiple cell types and within multiple tissues ($P = 0.01$, permutation of pairwise distance matrix). TCRs shared between mice within multiple tissue and T-cell types distinguish between lean and obese mice. Diet-dependent repertoire similarity is observed in liver in addition to AT. *C*: $CD8^+$ T-cell repertoires from liver and AT reflect simultaneous clonal expansion and sharing within each mouse and show that diet significantly affects repertoire similarity within the $CD8^+$ compartment ($P < 0.05$, permutation of pairwise distance matrix). A, AT; L, liver.

Regardless of dietary condition and tissue type, we identified 15,419 TCRs shared between any two samples, 9,034 TCRs shared between any two $CD8^+$ liver samples, 1,126 TCRs shared between any two $CD4^+$ AT samples, and 826 TCRs shared between any two $CD8^+$ AT samples (Supplementary Data). We also detected previously reported clonotypes that have been associated with obesity and IR in mouse models in both LFD- and HFD-fed mice (Table 1).

HFD Alters Physicochemical Properties of the TCR Repertoire

In addition to being more clonal, the TCR repertoire of mice fed an HFD demonstrated marked physicochemical differences from mice fed an LFD. To assess these differences, we systematically compared the CDR3 of every TCR detected in LFD- and HFD-fed mice and $CD4^+$ to $CD8^+$ TCRs. Obesity resulted in an elevation in charge ($P = 0.01$) (Fig. 5*A*) and a decrease in polarity in $CD8^+$ TCRs from AT ($P < 0.05$) (Fig. 5*B*). These repertoire-level changes do not appear to originate from germline selection and instead derive from the junctional regions of the CDR3, where TCR diversity is generated at the nucleotide level (Fig. 5*C* and *D*).

To examine more closely the differences in charge and polarity, we used sequence entropy measurements to detect enriched and depleted amino acids in the CDR3s of $CD8^+$. Weighted Shannon entropy (Fig. 6*A*) and Kullback-Leibler divergence (Fig. 6*B*) demonstrated that these changes are due to an enrichment of arginine and depletion of negatively charged amino acids, with other positively charged amino acids selected for at positions 8, 9, and 11. Unweighted Shannon entropy (Fig. 6*C*) and Kullback-Leibler divergence (Fig. 6*D*), where each TCR is given equal weight, revealed that both lysine and histidine contribute strongly to the increase in charge observed.

HFD Leads to isoLG Accumulation in ATMs

The physicochemical alterations in the $CD8^+$ TCR repertoires of HFD-fed mice led us to consider how the CDR3 of the TCRβ chain could interact with the local biochemical environment of AT. Because we observed an increased charge

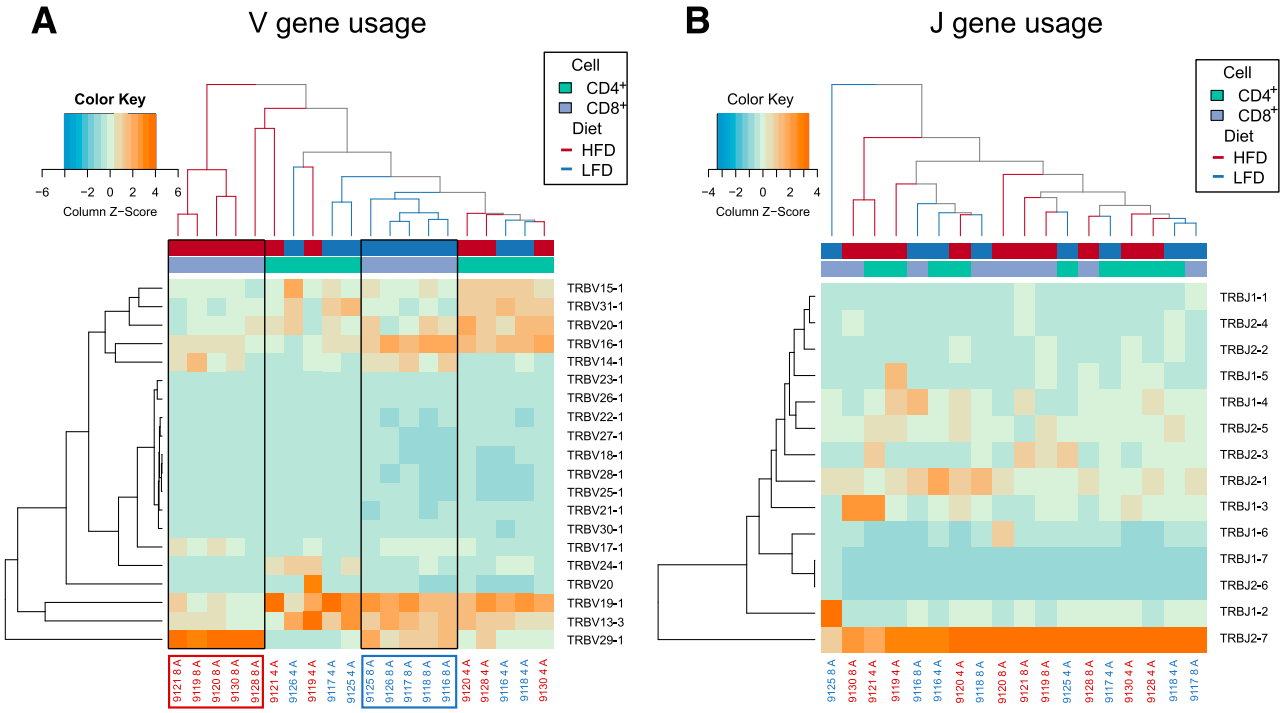

Figure 4—CD8+ TCR repertoires within AT are genetically distinct by dietary group. *Z*-score–normalized heat maps were built using VDJTools. Labels underneath the heat maps correspond to individual mice, and rows correspond to a given Vβ (TRBV) gene. The heat map is colored on the basis of *Z*-score and how many SDs from the mean a given sample is in its expression of a given Vβ gene family. *A*: Obesity leads AT CD8+ T cells to use distinct sets of V gene segments. These changes do not appear to distinguish between CD4+ T cells of lean and obese mice, although CD4+ T cells appear to use different sets of Vβ genes than CD8+ T cells regardless of dietary condition. *B*: Obesity does not affect the J segments used within the CD8+ TCR repertoires of mice to the same extent that V segments do. This is unsurprising because there are fewer Jβ (TRBJ) genes than Vβ genes and because the Jβ region frequently accounts for less nucleotide diversity than the Vβ region.

and decreased polarity, we chose to examine the isoLG content of APCs within AT because these highly reactive γ-ketoaldehydes carry both negatively charged phospholipid content and nonpolar lipid content (Fig. 7*A*). IsoLGs have been shown to rapidly adduct to lysines on self-proteins, forming isoLG protein adducts that are processed and presented as neoantigens, and induce an autoimmune-like state in hypertension (11). We isolated total leukocytes from AT and performed flow cytometry to identify isoLG protein adducts in ATMs (Fig. 7*A*). As previously reported by other research groups (32,33), HFD increased total ATM density and ATM subsets CD11c+ (M1-like ATMs), CD206+ (M2-like ATMs), and double-positive populations (Supplementary Fig. 2*B* and *C*). After HFD, ATMs showed increased isoLG-adduct formation (Fig. 7*B*) and expression of the costimulatory molecule B7 ligand CD86 (Fig. 7*C*). Regardless of ATM polarization state, HFD led to significant elevations of isoLGs in the number of cells per gram of AT of CD11c+, CD206+, and CD11c+CD206+ ATMs compared with LFD (Fig. 7*D*–*F*). However, HFD only increased the percentage of isoLG+ cells in CD206+ ATMs (Fig. 7*E*).

Because HFD led to elevations in isoLGs in ATMs, we sought to determine whether isoLGs in macrophages induce T-cell activation. As a control and to verify that isoLG-containing macrophages activate T cells, we treated BMDMs with 1 mmol/L TBHP, which induces oxidative stress. Treatment with TBHP led to elevations in isoLGs in BMDMs (Fig. 8*A* and *B*) and as previously reported (11). With use of an in vitro coculture system, we polarized BMDMs to M1, M2, and obesogenic MMes to represent the various subsets present in AT during HFD. Of note, isoLG levels were elevated only in M2-polarized macrophages compared with M0 ($P < 0.05$), were lower in M1 macrophages ($P < 0.001$), and were not different in MMes compared with M0 (Fig. 8*A* and *B*). TBHP-treated and polarized BMDMs were subsequently cultured with pan-T cells isolated from spleens of LFD- and HFD-fed mice. As expected, coculture with TBHP-treated macrophages led to elevations of total CD8+ T cells (Fig. 8*C*) and more specifically in activated cells as indicated by expression of the early activation marker CD69 (Fig. 8*D*). Furthermore, only the isoLG-containing M2 macrophages promoted an increase in CD8+ T cells and their activation (Fig. 8*C* and *D*), and this was only when cocultured with CD8+ T cells from the obese HFD-fed mice. Together, these findings demonstrate that ATMs express isoLGs under obese conditions and that isoLG-containing M2 macrophages are capable of driving CD8+ T-cell activation in vitro.

DISCUSSION

We demonstrate that HFD-fed mice have a higher AT CD8+ T-cell density and TCR clonality. CD8+ cells from AT of HFD-fed mice also have a distinctive TCR repertoire that differs in both charge and polarity within the CDR3 region

Table 1—Detection of previously reported T-cell clonotypes associated with pathogenesis in mouse models of obesity and diabetes

CDR3 AA	Reference	HFD Liver CD8	HFD Adipose CD8	HFD Adipose CD4	LFD Liver CD8	LFD Adipose CD8	LFD Adipose CD4	Annotation	*P* value
CASSLGSGNTLYF	26	4	1	1	3	0	0	Expanded in pancreas	NS
CASSDAGQYEQYF	26	1	0	0	2	0	0	Expanded in pancreas	NS
CASSDSAETLYF	26	3	3	0	1	0	0	Expanded in pancreas	*
CASGDEGYEQYF	26	1	0	1	0	0	0	Expanded in pancreas	NS
CASGDAREQYF	26	2	1	0	3	0	0	Expanded in pancreas and B-cell scaffolds	NS
CASGSSYEQYF	26	2	0	1	2	0	0	Expanded in β-cell scaffolds	NS
CASSDAGTTNERLFF	26	1	0	1	0	0	0	Expanded in β-cell scaffolds	NS
CASGSSYEQYF	26	2	0	1	2	0	0	Expanded in β-cell scaffolds	NS
CASSLGTGDEQYF	27	2	1	1	1	0	1	Diabetogenic clone BDC 4.12	NS
CASSGTGGQNTLYF	28	0	0	0	3	0	0	Diabetogenic clone AI15.A3, β-cell autoreactive	*
CASSGTGGQNTLY	28	0	0	0	3	0	0	Diabetogenic clone AI5.F5, β-cell autoreactive	*
CASSLGGYEQYF	29	3	1	3	5	1	2	Proinsulin reactive	NS
CASSRDNTEVF	29	3	0	1	2	0	0	Insulin reactive	NS
CASSLTGNTGQLY	29	2	0	4	1	0	0	Insulin reactive	*
CASSPDNYEQY	29	1	1	1	2	0	0	Insulin reactive	NS
CASSRHQDTQYF	30	1	0	0	2	0	0	Specificity not known	NS
CASSLGGYEQY	31	3	1	2	5	1	2	Reactive against insulin	NS

*$P \leq 0.05$.

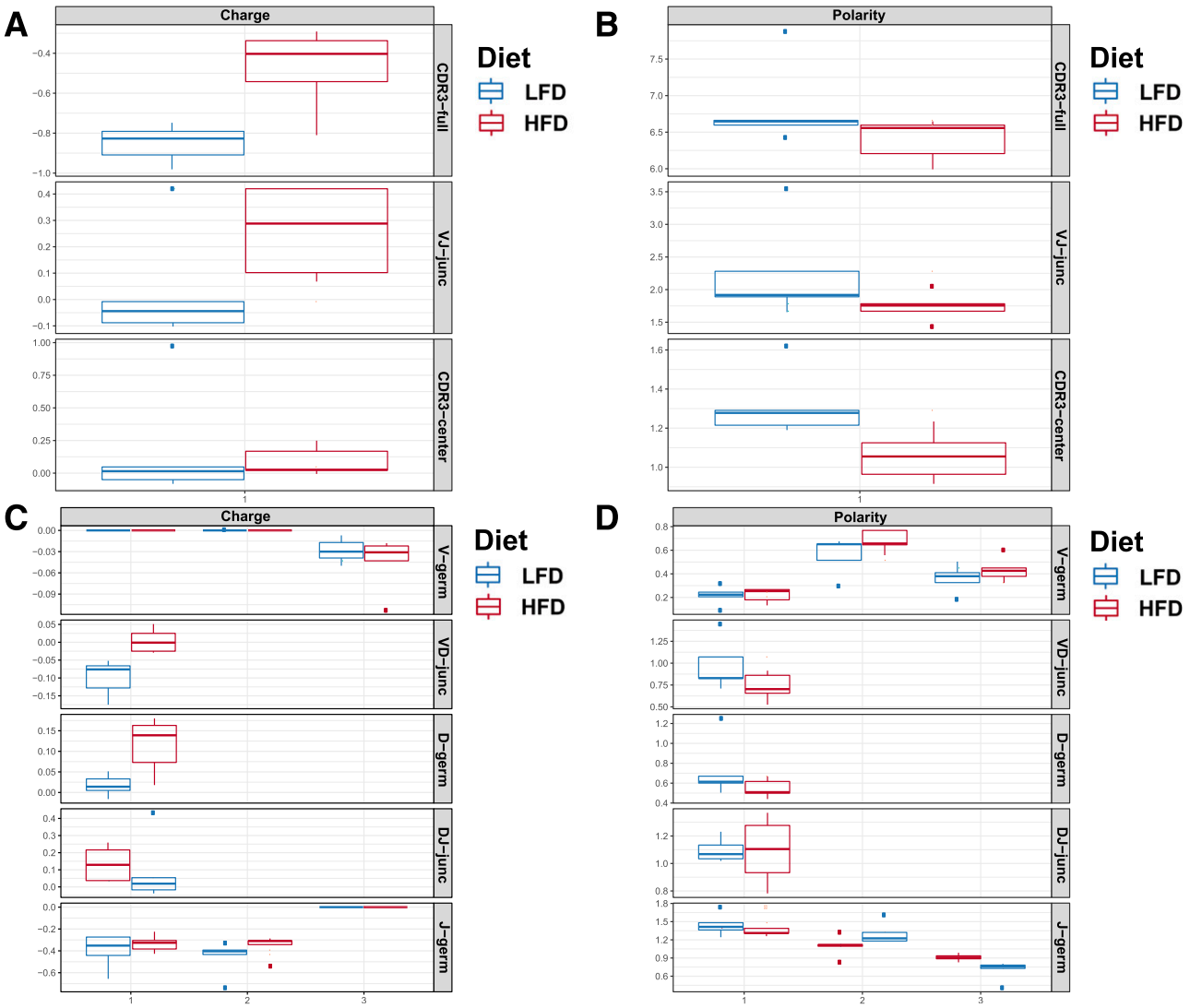

Figure 5—CD8+ TCR repertoires of mice fed an HFD differ in physicochemical properties compared with those of mice fed an LFD. *A*: AT CD8+ T-cell repertoires of obese mice are significantly higher in charge ($P = 0.01$, Student *t* test). This elevation in charge is due to amino acids encoded in the junctional regions of the TCR, where diversity is generated. *B*: The CD8+ T-cell repertoire within AT also is markedly lower in polarity in obese mice ($P < 0.01$, Student *t* test). Unlike the changes observed in charge, the difference in polarity appears to arise from germline selection. *C*: Elevations in charge arise from the junctional regions of the TCR, where TCR diversity is generated at the nucleotide level. Repertoires were assessed using three scanning bins to account for variance along each region and to identify signal arising from each genetic region of the TCR. *D*: The increased polarity of AT CD8+ TCR repertoires from obese mice appears to be more closely related to changes selected at the germline level, unlike changes in charge. germ, germline; junc, junction.

compared with LFD-fed mice. These changes are not observed within the CD4+ TCR repertoire, which uses different V-segment genes than CD8+ T cells, regardless of diet (Fig. 4*A*). The repertoires of mice fed an HFD are also more public than of mice fed an LFD, which has been reported previously in autoimmune pathologies but uncommonly in antipathogen responses (reviewed in Madi et al. [34]). Furthermore, we provide evidence that these repertoire properties may emerge in part as a response to an increase in immunogenic isoLG adducts present in the ATMs of mice fed an HFD. We have directly identified and quantitated specific clonally expanded TCRs within the CD8+ and CD4+ T-cell populations that appear to arise in response to DIO. We also demonstrate that the AT TCR repertoire alone can distinguish between LFD- and HFD-fed mice. To that end, we note that HFD induces repertoire-level changes previously described in studies of autoimmunity and enriches for amino acid sequences biased toward a positive charge. In fact, Glanville et al. (35) recently described a strong inverse correlation between CDR3 charge and epitope charge in TCRs of both humans and mice. Finally, we document elevated numbers of isoLG-positive macrophages in the AT of HFD-fed mice and that M2 macrophages containing isoLG-adducted protein enhance T-cell survival and activation. These data suggest a coordinated mechanism of inflammation within

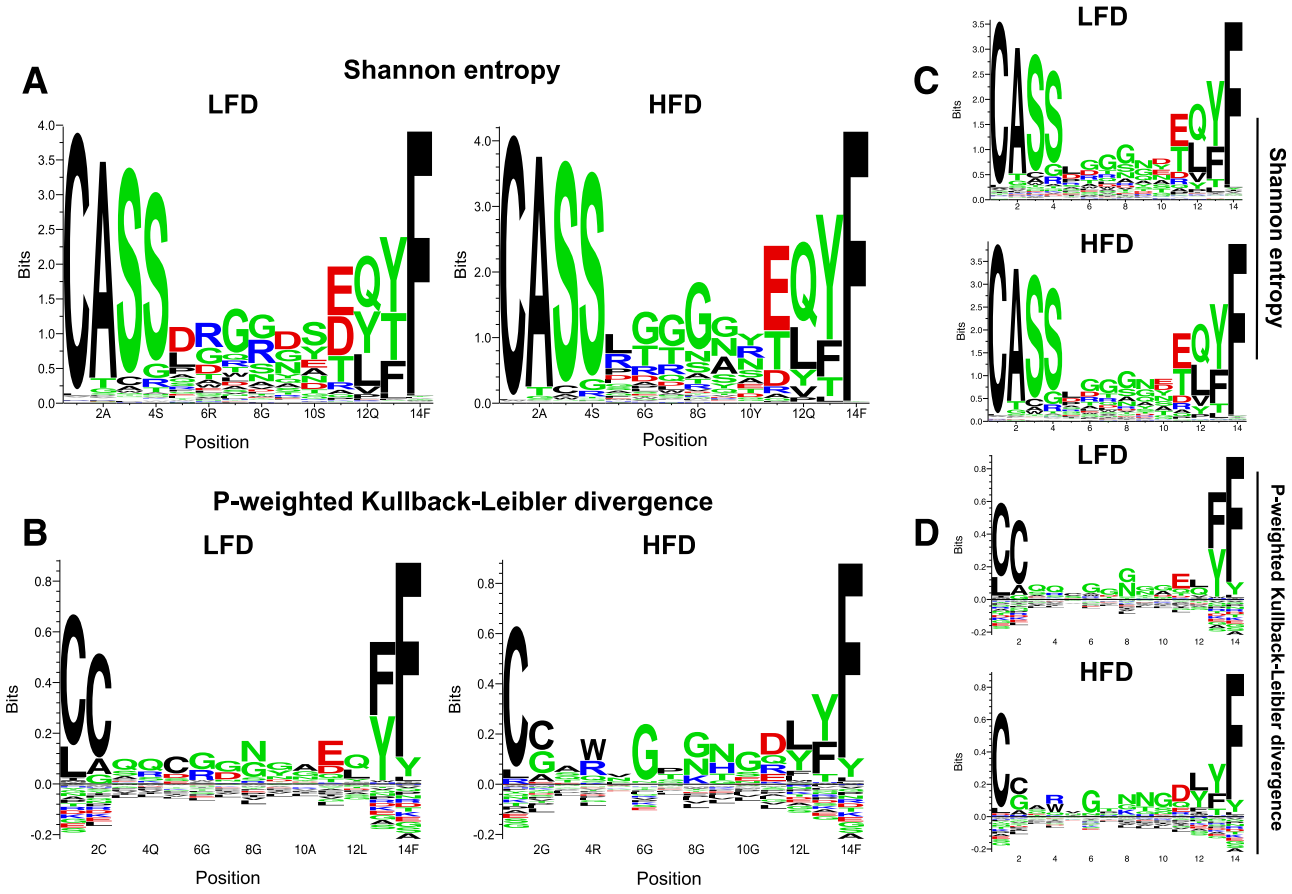

Figure 6—Weighted and unweighted measures of entropy demonstrate selection for positively charged amino acids within the CDR3 of HFD TCR repertoires. The median CDR3 length was 14 amino acids, which we analyzed using several sequence entropy methods. *A*: Shannon entropy reveals enrichment of arginine and depletion of negatively charged amino acids in the CD8$^+$ repertoires of HFD-fed mice. *B*: P-weighted Kullback-Leibler divergence with Hobohm1 clustering reveals that other positively charged amino acids are enriched within HFD CD8$^+$ TCR repertoires from AT and that negatively charged amino acids are correspondingly depleted. *C* and *D*: Unweighted analyses using Shannon entropy (*C*) and P-weighted Kullback-Leibler divergence (*D*) show that these amino acid enrichments are due to clonotypes present at higher frequencies, although there is still enrichment for arginine, lysine, and histidine, all of which carry a positive charge at physiological pH. This indicates that obesity-induced changes in charge and polarity at the repertoire level are driven not only by highly expanded clonotypes but also by clonotypes that are present at lower frequencies.

AT wherein T cells infiltrate tissue in response to neoantigen presented on ATMs.

To date, other studies have described the infiltration of a possibly clonally expanded T-cell population within AT (4,7,10,36). In mice, Yang et al. (9) observed shifts in the clonality of both the AT CD4$^+$ and CD8$^+$ TCR repertoires in obese versus lean mice using PCR-based spectratyping, where clonal expansion was detected as a deviation from the normally Gaussian frequency distribution of CDR3 length. Although spectratyping has been advantageous in the detection of unusual T-cell clones in lymphoma, it does not provide the specificity or direct measurement of clonal expansion and cannot distinguish between expanded clones with different amino acid sequences and similar V and J gene usage. Consequently, spectratyping also cannot detect clones with identical amino acid sequences and different V and J gene usage, as we observed in the CD8$^+$ and CD4$^+$ TCR repertoires of mice fed both an LFD and an HFD (Supplementary Data). In contrast, deep sequencing of the TCR repertoire makes it possible to distinguish between the TCR repertoires of LFD- or HFD-fed mice (Fig. 3) and to assess intricate biochemical details of the TCR at the repertoire level (Figs. 4–6). Similar observations have been made with regard to HFD-induced T-cell infiltration in pancreatic islets (30,37–39,40), skeletal muscle (41), and liver (42). We observed similar levels of macrophage and CD8$^+$ T-cell infiltration as reported in prior studies and further identified several highly oligoclonal CD8$^+$ T-cell populations induced by HFD. As previously reported by Nishimura et al. (4), we observed no difference in CD4$^+$ T-cell infiltration into AT and extend this observation to include no significant difference in CD4$^+$ T-cell clonality (P = 0.18). Although we do not observe enrichment of Vβ gene families 7 and 10b as in Nishimura et al., we do observe slight enrichment of Vβ families 17, 18, 21, 22, 25, 27, 28, and 29 (Fig. 4*A*). We observe a pronounced increase in the

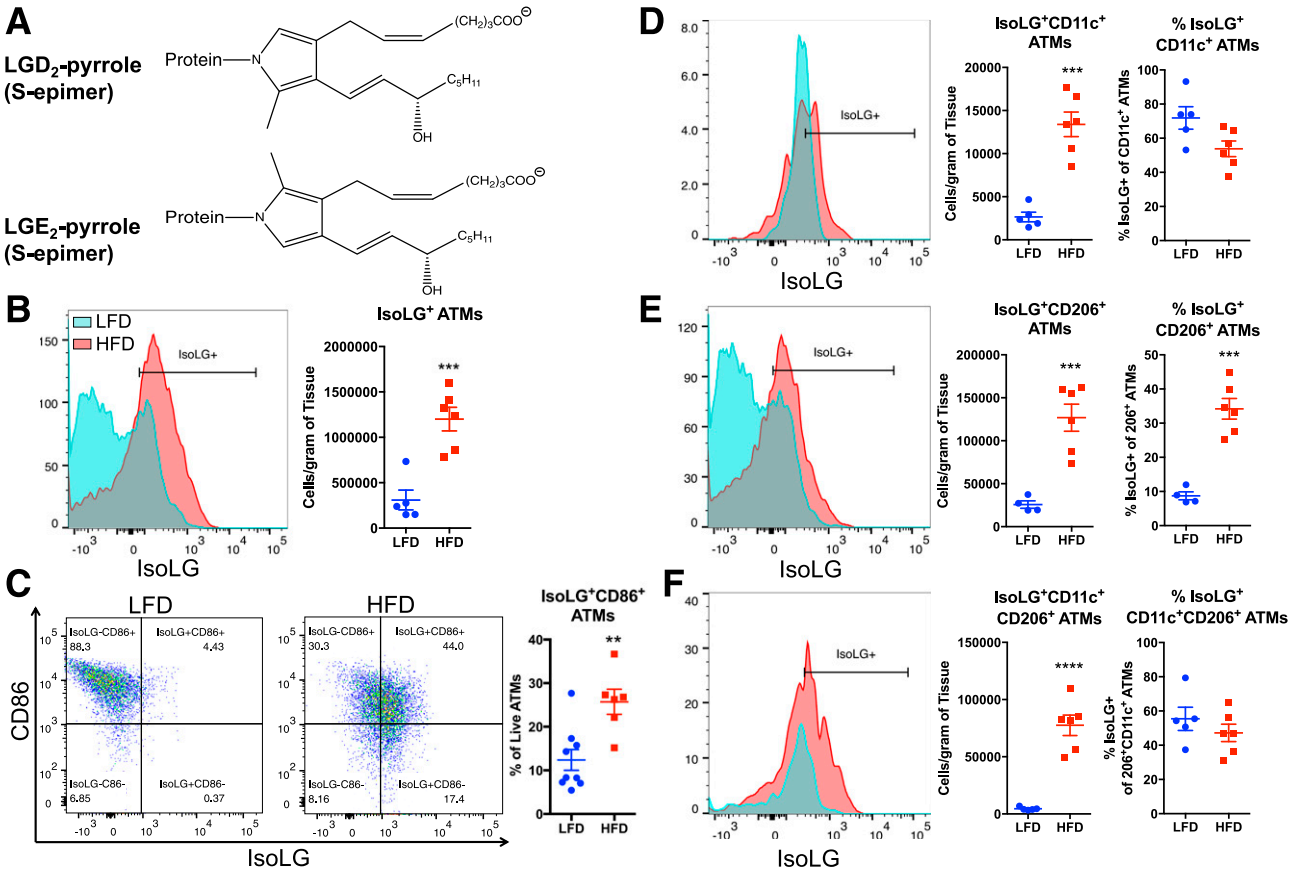

Figure 7—HFD induces formation of immunogenic isoLGs and expression of B7 ligand CD86 in ATMs. Total leukocytes were isolated from AT of mice fed an LFD or HFD, and isoLG content was quantified using previously described gating schema. *A*: Structure of the major isoLG protein adducts. The major intermediates are a pair of pyrrolic epimers whose covalently bonded nitrogen originates from lysine residues on proteins. Phospholipids attached to isoLGs derive from polyunsaturated acids, arachidonic acids, and phospholipids thereof. *B*: Representative flow cytometry plot and average data showing intracellular staining for isoLG protein adducts in ATMs using the single-chain antibody D-11 single-chain variable fragment. *C*: Representative FACS plots and average data showing surface expression of CD86 and isoLGs in ATMs (proportion of ATMs staining $CD86^+isoLG^+$). *D–F*: Representative flow cytometry plots and average data showing the number of $isoLG^+$ cells per gram of tissue and percentage of $isoLG^+$ cells per ATM subsets $CD11c^+$ (*D*), $CD206^+$ (*E*), and $CD11c^+CD206^+$ (*F*) of HFD-fed mice. Data are mean ± SEM (n = 5−10 mice/group). $^{**}P < 0.01$, $^{***}P < 0.001$, $^{****}P < 0.0001$.

clonality of $CD8^+$ T cells in AT of HFD-fed mice and note that future studies should specifically examine the extent to which this is induced by diet alone or entirely depends on obesity. Future dietary studies also would benefit from analysis of age because at least one study indicated that AT mass and $CD8^+$ T cells—but not $CD4^+$ T cells—are elevated independent of diet in aging male and female mice (43).

Highly clonal T-cell populations have been described in a broad array of pathologies (44). Our group has demonstrated recently that the TCR repertoire is more clonal in the AT of obese and overweight adults with HIV infection receiving long-term therapy than in the blood and that the V-J gene family pairings appear to differ between tissue compartments (36), suggesting that similar repertoire contraction also occurs in the AT of humans. Adverse effects of similarly clonal populations have been described in both obesity and diabetes. Highly clonal T-cell populations recognizing an HLA-DR4–restricted epitope of insulin have been documented in patients with type 1 diabetes (45). Obesity in both mice and humans leads to markedly lower naive T-cell pools and highly clonal T-cell populations, further restricting the availability of diverse TCRs (46). A recent report by Pham et al. (2) indicated that HFD also limits the diversity of the B-cell repertoire, which corresponds with IR. The presence of a clonally expanded T-cell population within tissue can be explained by several immunological processes. One possible scenario is that a T-cell population may infiltrate in response to an antigen within the tissue, as documented in the AT of humans and macaques during chronic simian immunodeficiency viral and HIV infection (47). Another is the presence of multiple T-cell populations sharing the same TCR but with drastically different functional roles and properties (48). Alternatively, dominant clones from the blood could enter the tissue in an antigen-blind fashion.

Our findings raise the question of where and how antigen is presented to drive TCR clonal expansion. Several

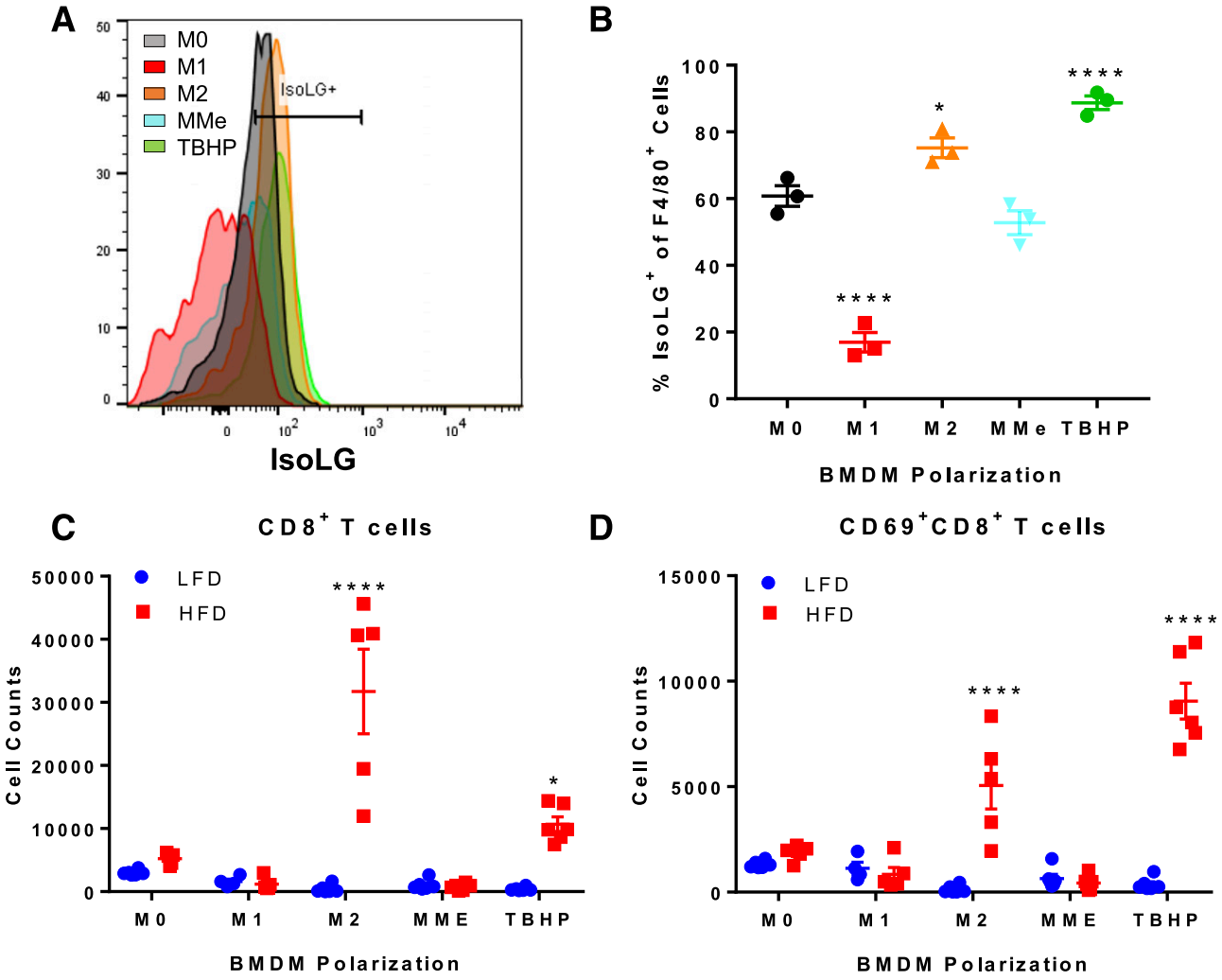

Figure 8—M2 polarization increases IsoLGs levels and promotes activation of $CD8^+$ T cells. BMDMs were polarized to M0, M1, M2, or MMe or treated with TBHP. After polarization, BMDMs were cocultured with isolated T cells from the spleen of mice fed an LFD or HFD for 3 days. IsoLG content was quantified in polarized BMDMs by flow cytometry. *A* and *B*: Flow analysis (*A*) and quantification (*B*) of $IsoLG^+$ $F4/80^+$ cells (one-way ANOVA). Data are mean ± SEM (n = 3 wells/group). T cells were collected from cocultures, and flow analysis was performed to quantify $CD8^+$ T cells (*C*) and $CD8^+CD69^+$ T cells (*D*) (two-way ANOVA). Data are mean ± SEM (n = 5 mice/LFD or HFD group) and mean ± SEM (n = 5 wells/group). $^*P \leq 0.05$, $^{****}P \leq 0.0001$.

published reports have indicated that antigen presentation to $CD4^+$ T cells occurs directly in AT. Multiple MHC-II–expressing APC populations in AT can present to $CD4^+$ T cells, including B cells (3), dendritic cells (49), macrophages (50), and even adipocytes (51). Mice with global deficiency of MHC-II demonstrate protection from AT inflammation and systemic IR when placed on an HFD (50). A portion of the reduced inflammation in AT was due to attenuation of $CD11c^+$ macrophages and $CD4^+$ T-cell accumulation (50). Adipokines also can activate these APCs directly, including leptin, adiponectin, and retinol-binding protein 4 (51–53). Thus, AT has all the prerequisite components to activate $CD4^+$ T cells. However, our studies show clonality in the $CD8^+$ T-cell population, begging the question of their activation signals. MHC-I is expressed on all cell types and could allow for presentation of neoantigens or modified proteins. The current data suggest an enrichment of arginine and positively charged amino acids in the TCRs of $CD8^+$ T cells that are clonally expanded in HFD-fed mice. This positive charge led us to consider that protein modifications leading to a negative charge might serve as neoantigens in AT. Indeed, the data suggest that ATMs display increased levels of isoLG adducts (Fig. 7). Similar alterations in charge and amino acid content have been reported in the context of renal disease (11,54). Insulin-reactive TCRs have been reported to be enriched for arginine and for nonpolar amino acids at position 7 (55), which we also observed. We identified TCRs previously associated with obesity and IR in mice (Table 1), two of which were significantly enriched in HFD TCR repertoires. One clonotype that was highly prevalent in AT is known to be insulin reactive, and another is known to be enriched in the pancreas of diabetic mice. In contrast, two previously reported diabetogenic clonotypes were

detected at elevated levels in LFD-fed mice alone (Table 1), which demonstrates that changes to the TCR repertoire extend to multiple tissues in the context of obesity and IR and that insulin reactivity alone may not explain clonal expansion within AT. Although we did not observe significant changes in the TCR repertoire of $CD4^+$ T cells of the AT, future studies also could examine the TCR repertoire of $CD4^+$ T cells within the liver, where fat also accumulates during DIO.

The current findings suggest that isoLGs may act as neoantigens responsible for AT TCR clonal expansion. Generation of these reactive lipid aldehydes primarily depends on oxidative stress, and reactive lipid aldehydes are detected at elevated levels in other autoimmune processes, including multiple sclerosis, glaucoma, allergic inflammation, and cancer (reviewed in Salomon and Bi [56]). Previous studies examined the role of various lipid adducts on the immunogenicity of APCs and found that only proteins adducted to isoLGs induced APC immunogenicity (11). A number of reports demonstrated that oxidative stress levels are elevated in AT of obese mice and humans (57,58). In pulmonary injury, impaired NADPH oxidase reduces production of isoLG-adducted proteins, whereas impairment of the Nrf2-antioxidant response element signaling pathway increases isoLG-modified protein levels (59). Furthermore, inhibition of NADPH oxidase reduces obesity-induced AT reactive oxygen species production, inflammation, and IR (57,58). Thus, obesity-induced oxidative stress in ATMs may account for the elevation in isoLGs.

Although our results suggest that M2-like ATMs induce or enhance clonal expansion of AT-infiltrating T cells through the presentation of immunogenic isoLG-adducted peptides, the extent to which ATM-generated isoLGs induce clonal expansion in T cells remains to be explored. We also note that T cells derived from splenocytes in the liver may not precisely reflect those found in AT and that a culture model able to effectively enrich such lymphocytes from the AT would be a valuable contribution to the field. The current results also suggest several new directions for further investigation. The antigen specificity of clonally expanded T cells within AT remains to be determined, and single-cell TCR sequencing can connect surface phenotype information from flow cytometry with transcriptomics and paired TCRα/β sequences (60). Although we did not identify any clonotypes that were universally shared at high (>1%) frequencies between or within diet groups, we did observe several TCRs that were shared within the top 100 clonotypes of each dietary group (Table 1 and McDonnell [62]), particularly with respect to HFD-fed mice. This suggests that the antigens or neoantigens presented in obesity may not be the same from mouse to mouse. These TCRs may be specific for one or more antigens, although we have previously shown that T_H1 $CD4^+$ cells, $CD8^+$ T cells, and memory cells accumulate in the AT of weight-cycled mice, suggesting secondary immune responses with repeat exposure to HFD (61), and our in vitro experiments suggest that isoLG-containing macrophages augment T-cell activation and survival in tissue-resident immune populations that are expanded in obesity (Fig. 8).

In summary, we have demonstrated that T cells infiltrating AT of obese mice are clonally expanded, that the TCR repertoires of lean and obese mice are distinct in their sequences and biochemical properties, that immunogenic isoLGs are elevated in ATMs of obese mice, and that T cells of obese mice accumulate and activate in response to isoLG-containing M2 macrophages. Our observations also suggest that therapy targeting the $CD8^+$ T-cell population and antigens thereof could potentially abrogate inflammation and other consequences of adaptive immune activation in obesity.

Funding. This study was supported by Tennessee Center for AIDS Research grant P30-AI-110527. TCR sequencing was performed in the Vanderbilt Technologies for Advanced Genomics Core laboratory. W.J.M. was supported by funding from National Institutes of Health T32 award HL-069765 and is supported by R01 award DK-112262. J.R.K. was supported by K23 award AI-100700-06 and is supported by R01 award DK-112262. M.A.C. is supported by funding from T32 award DK-007563. This work was supported by a Merit Award from the Veterans Affairs Tennessee Valley Healthcare System (5I01BX002195) to A.H.H., who is also supported by an Innovation Award from the American Diabetes Association (1-17-IBS-140). Flow cytometry was performed in the Vanderbilt Medical Center Flow Cytometry Core shared resource, supported by the Vanderbilt Ingram Cancer Center (CA-68485) and the Vanderbilt Digestive Disease Research Center (DK-058404), from which A.H.H. received a scholarship. A.J.K. is supported by National Heart, Lung, and Blood Institute K01 award HL-121010.

The funders played no role in the study design, data collection and analysis, decision to publish, or preparation of the manuscript.

Duality of Interest. No potential conflicts of interest relevant to this article were reported.

Author Contributions. W.J.M. performed the software analysis. W.J.M., J.R.K., S.A.M., M.A.P., A.K., M.K.A., M.A.C., A.H.H., and A.J.K. contributed to the writing, review, and editing of the manuscript. W.J.M., J.R.K., S.A.M., M.A.P., A.H.H., and A.J.K. contributed to the study concept and methodology. W.J.M., J.R.K., A.K., M.K.A., M.A.C., A.H.H., and A.J.K. validated the data. W.J.M., J.R.K., A.H.H., and A.J.K. curated the data and drafted the manuscript. W.J.M., J.R.K., and A.J.K. performed the formal analysis. W.J.M., M.A.P., A.K., M.K.A., M.A.C., and A.J.K. performed the investigation. W.J.M. and A.J.K. contributed to the visualization. J.R.K., S.A.M., and A.H.H. provided resources. J.R.K., S.A.M., A.H.H., and A.J.K. supervised the project, provided project administration, and acquired funding. W.J.M. and A.J.K. are the guarantors of this work and, as such, had full access to all the data in the study and take responsibility for the integrity of the data and the accuracy of the data analysis.

Prior Presentation. Parts of this study were presented in abstract form at the Inaugural Immunometabolism and Chronic Diseases Conference, Coral Coast, Fiji, 13–16 August 2017; the 17th International Winter Eicosanoid Conference, Baltimore, MD, 11–13 March 2018; and the 7th Annual Southeastern Immunology Symposium, Birmingham, AL, 16–17 June 2018.

Data Availability. The data that support the findings of this study are available from A.J.K. upon request.

References

1. Kohlgruber AC, LaMarche NM, Lynch L. Adipose tissue at the nexus of systemic and cellular immunometabolism. Semin Immunol 2016;28:431–440

2. Pham TD, Chng MHY, Roskin KM, et al. High-fat diet induces systemic B-cell repertoire changes associated with insulin resistance. Mucosal Immunol 2017;10:1468–1479

3. Winer DA, Winer S, Shen L, et al. B cells promote insulin resistance through modulation of T cells and production of pathogenic IgG antibodies. Nat Med 2011; 17:610–617
4. Nishimura S, Manabe I, Nagasaki M, et al. CD8+ effector T cells contribute to macrophage recruitment and adipose tissue inflammation in obesity. Nat Med 2009;15:914–920
5. Duffaut C, Galitzky J, Lafontan M, Bouloumié A. Unexpected trafficking of immune cells within the adipose tissue during the onset of obesity. Biochem Biophys Res Commun 2009;384:482–485
6. Feuerer M, Herrero L, Cipolletta D, et al. Lean, but not obese, fat is enriched for a unique population of regulatory T cells that affect metabolic parameters. Nat Med 2009;15:930–939
7. Winer S, Chan Y, Paltser G, et al. Normalization of obesity-associated insulin resistance through immunotherapy. Nat Med 2009;15:921–929
8. Stolarczyk E, Vong CT, Perucha E, et al. Improved insulin sensitivity despite increased visceral adiposity in mice deficient for the immune cell transcription factor T-bet. Cell Metab 2013;17:520–533
9. Yang H, Youm YH, Vandanmagsar B, et al. Obesity increases the production of proinflammatory mediators from adipose tissue T cells and compromises TCR repertoire diversity: implications for systemic inflammation and insulin resistance. J Immunol 2010;185:1836–1845
10. Correia-Neves M, Waltzinger C, Mathis D, Benoist C. The shaping of the T cell repertoire. Immunity 2001;14:21–32
11. Kirabo A, Fontana V, de Faria AP, et al. DC isoketal-modified proteins activate T cells and promote hypertension. J Clin Invest 2014;124:4642–4656
12. Orr JS, Kennedy AJ, Hasty AH. Isolation of adipose tissue immune cells. J Vis Exp 2013;(75):e50707
13. Robins H, Desmarais C, Matthis J, et al. Ultra-sensitive detection of rare T cell clones. J Immunol Methods 2012;375:14–19
14. Trouplin V, Boucherit N, Gorvel L, Conti F, Mottola G, Ghigo E. Bone marrow-derived macrophage production. J Vis Exp 2013;(81):e50966
15. Hill AA, Anderson-Baucum EK, Kennedy AJ, Webb CD, Yull FE, Hasty AH. Activation of NF-κB drives the enhanced survival of adipose tissue macrophages in an obesogenic environment. Mol Metab 2015;4:665–677
16. Shugay M, Bagaev DV, Turchaninova MA, et al. VDJtools: unifying post-analysis of T cell receptor repertoires. PLOS Comput Biol 2015;11:e1004503
17. Nazarov VI, Pogorelyy MV, Komech EA, et al. tcR: an R package for T cell receptor repertoire advanced data analysis. BMC Bioinformatics 2015;16: 175
18. Krijthe JH. Rtsne: T-distributed stochastic neighbor embedding using a Barnes-Hut implementation [Internet], 2015. Available from https://github.com/jkrijthe/Rtsne. Accessed 18 September 2018
19. Suzuki R, Shimodaira H. Pvclust: an R package for assessing the uncertainty in hierarchical clustering. Bioinformatics 2006;22:1540–1542
20. Ripley BD, Venables WN. *Modern Applied Statistics With S-PLUS*. Berlin, Germany, Springer Science & Business Media, 2013
21. Feoli E, Orlóci L. Analysis of concentration and detection of underlying factors in structured tables. Vegetatio 1979;40:49–54
22. Williams EJ. Use of scores for the analysis of association in contingency tables. Biometrika 1952;39:274–289
23. Thomsen MC, Nielsen M. Seq2Logo: a method for construction and visualization of amino acid binding motifs and sequence profiles including sequence weighting, pseudo counts and two-sided representation of amino acid enrichment and depletion. Nucleic Acids Res 2012;40:W281–W287
24. Candéias S, Waltzinger C, Benoist C, Mathis D. The V beta 17+ T cell repertoire: skewed J beta usage after thymic selection; dissimilar CDR3s in CD4+ versus CD8+ cells. J Exp Med 1991;174:989–1000
25. Emerson R, Sherwood A, Desmarais C, Malhotra S, Phippard D, Robins H. Estimating the ratio of CD4+ to CD8+ T cells using high-throughput sequence data. J Immunol Methods 2013;391:14–21
26. Thelin MA, Kissler S, Vigneault F, et al. In vivo enrichment of diabetogenic T cells. Diabetes 2017;66:2220–2229
27. Candéias S, Katz J, Benoist C, Mathis D, Haskins K. Islet-specific T-cell clones from nonobese diabetic mice express heterogeneous T-cell receptors. Proc Natl Acad Sci U S A 1991;88:6167–6170
28. DiLorenzo TP, Graser RT, Ono T, et al. Major histocompatibility complex class I-restricted T cells are required for all but the end stages of diabetes development in nonobese diabetic mice and use a prevalent T cell receptor alpha chain gene rearrangement. Proc Natl Acad Sci U S A 1998;95:12538–12543
29. Pearson JA. Analysis of the Repertoire of Insulin-Reactive CD8+ T Cells. Cardiff, UK, Cardiff University, 2014
30. Lennon GP, Bettini M, Burton AR, et al. T cell islet accumulation in type 1 diabetes is a tightly regulated, cell-autonomous event. Immunity 2009;31:643–653
31. Pearson JA, Thayer TC, McLaren JE, et al. Proinsulin expression shapes the TCR repertoire but fails to control the development of low-avidity insulin-reactive CD8+ T cells. Diabetes 2016;65:1679–1689
32. Nawaz A, Aminuddin A, Kado T, et al. CD206$^+$ M2-like macrophages regulate systemic glucose metabolism by inhibiting proliferation of adipocyte progenitors. Nat Commun 2017;8:286
33. Li P, Lu M, Nguyen MT, et al. Functional heterogeneity of CD11c-positive adipose tissue macrophages in diet-induced obese mice. J Biol Chem 2010;285:15333–15345
34. Madi A, Shifrut E, Reich-Zeliger S, et al. T-cell receptor repertoires share a restricted set of public and abundant CDR3 sequences that are associated with self-related immunity. Genome Res 2014;24:1603–1612
35. Glanville J, Huang H, Nau A, et al. Identifying specificity groups in the T cell receptor repertoire. Nature 2017;547:94–98
36. Koethe JR, McDonnell W, Kennedy A, et al. Adipose tissue is enriched for activated and late-differentiated CD8+ T cells and shows distinct CD8+ receptor usage, compared with blood in HIV-infected persons. J Acquir Immune Defic Syndr 2018;77:e14–e21
37. Butcher MJ, Hallinger D, Garcia E, et al. Association of proinflammatory cytokines and islet resident leucocytes with islet dysfunction in type 2 diabetes. Diabetologia 2014;57:491–501
38. Brooks-Worrell B, Narla R, Palmer JP. Islet autoimmunity in phenotypic type 2 diabetes patients. Diabetes Obes Metab 2013;15(Suppl. 3):137–140
39. Sarikonda G, Pettus J, Phatak S, et al. CD8 T-cell reactivity to islet antigens is unique to type 1 while CD4 T-cell reactivity exists in both type 1 and type 2 diabetes. J Autoimmun 2014;50:77–82
40. Wang J, Tsai S, Shameli A, Yamanouchi J, Alkemade G, Santamaria P. In situ recognition of autoantigen as an essential gatekeeper in autoimmune CD8+ T cell inflammation. Proc Natl Acad Sci U S A 2010;107:9317–9322
41. Khan IM, Dai Perrard XY, Perrard JL, et al. Attenuated adipose tissue and skeletal muscle inflammation in obese mice with combined CD4+ and CD8+ T cell deficiency. Atherosclerosis 2014;233:419–428
42. Wolf MJ, Adili A, Piotrowitz K, et al. Metabolic activation of intrahepatic CD8+ T cells and NKT cells causes nonalcoholic steatohepatitis and liver cancer via cross-talk with hepatocytes. Cancer Cell 2014;26:549–564
43. Ahnstedt H, Roy-O'Reilly M, Spychala MS, et al. Sex differences in adipose tissue CD8+ T cells and regulatory T cells in middle-aged mice. Front Immunol 2018;9:659
44. Miles JJ, Douek DC, Price DA. Bias in the αβ T-cell repertoire: implications for disease pathogenesis and vaccination. Immunol Cell Biol 2011;89:375–387
45. Kent SC, Chen Y, Bregoli L, et al. Expanded T cells from pancreatic lymph nodes of type 1 diabetic subjects recognize an insulin epitope. Nature 2005;435:224–228
46. Yang H, Youm YH, Vandanmagsar B, et al. Obesity accelerates thymic aging. Blood 2009;114:3803–3812
47. Damouche A, Lazure T, Avettand-Fènoël V, et al. Adipose tissue is a neglected viral reservoir and an inflammatory site during chronic HIV and SIV infection. PLoS Pathog 2015;11:e1005153
48. Bilate AM, Bousbaine D, Mesin L, et al. Tissue-specific emergence of regulatory and intraepithelial T cells from a clonal T cell precursor. Sci Immunol 2016;1:eaaf7471
49. Cho KW, Zamarron BF, Muir LA, et al. Adipose tissue dendritic cells are independent contributors to obesity-induced inflammation and insulin resistance. J Immunol 2016;197:3650–3661

50. Cho KW, Morris DL, DelProposto JL, et al. An MHC II-dependent activation loop between adipose tissue macrophages and CD4+ T cells controls obesity-induced inflammation. Cell Rep 2014;9:605–617
51. Mattioli B, Straface E, Quaranta MG, Giordani L, Viora M. Leptin promotes differentiation and survival of human dendritic cells and licenses them for Th1 priming. J Immunol 2005;174:6820–6828
52. Jung MY, Kim H-S, Hong H-J, Youn B-S, Kim TS. Adiponectin induces dendritic cell activation via PLCγ/JNK/NF-κB pathways, leading to Th1 and Th17 polarization. J Immunol 2012;188:2592–2601
53. Moraes-Vieira PM, Yore MM, Dwyer PM, Syed I, Aryal P, Kahn BB. RBP4 activates antigen-presenting cells, leading to adipose tissue inflammation and systemic insulin resistance. Cell Metab 2014;19:512–526
54. Wu H, Zhang GY, Knight JF. T cell receptor BV gene usage in interstitial cellular infiltrates in active Heymann nephritis. Nephrol Dial Transplant 2001;16:1374–1381
55. Pearson JA, Thayer TC, McLaren JE, et al. Proinsulin expression shapes the TCR repertoire but fails to control the development of low-avidity insulin-reactive CD8+ T cells. Diabetes 2016;65:1679–1689
56. Salomon RG, Bi W. Isolevuglandin adducts in disease. Antioxid Redox Signal 2015;22:1703–1718
57. Den Hartigh LJ, Omer M, Goodspeed L, et al. Adipocyte-specific deficiency of NADPH oxidase 4 delays the onset of insulin resistance and attenuates adipose tissue inflammation in obesity. Arterioscler Thromb Vasc Biol 2017;37:466–475
58. Coats BR, Schoenfelt KQ, Barbosa-Lorenzi VC, et al. Metabolically activated adipose tissue macrophages perform detrimental and beneficial functions during diet-induced obesity. Cell Reports 2017;20:3149–3161
59. Mont S, Davies SS, Roberts Second LJ, et al. Accumulation of isolevuglandin-modified protein in normal and fibrotic lung. Sci Rep 2016;6:24919
60. Schober K, Busch DH. A synergistic combination: using RNAseq to decipher both T-cell receptor sequence and transcriptional profile of individual T cells. Immunol Cell Biol 2016;94:529–530
61. Anderson EK, Gutierrez DA, Kennedy A, Hasty AH. Weight cycling increases T-cell accumulation in adipose tissue and impairs systemic glucose tolerance. Diabetes 2013;62:3180–3188
62. McDonnell W. McDonnell et al 2018 supplementary TCRseq/immunoSEQ dataset [Internet], 2018. Available from https://figshare.com/articles/McDonnell_et_al_2018_supplementary_TCRseq_immunoSEQ_dataset/6752834. Accessed 20 September 2018